JOURNAL OF SOLID STATE CHEMISTRY 111, 276–282 (1994)

Structure Determination and Magnetic Susceptibility of $Gd_{2/3}Cr_2S_4$

A. Meerschaut, A. Lafond, L. M. Hoistad, and J. Rouxel

Institut des Matériaux de Nantes, UMR-CNRS 110, Laboratoire de chimie des solides, 2, rue de la Houssinière, 44072 Nantes Cedex 02, France

Received June 29, 1993; in revised form September 27, 1993; accepted September 29, 1993

Besides the $(GdS)_{1.27}CrS_2$ misfit layered compound, gadolinium forms another compound with chromium and sulfur with the formulation $Gd_{2/3}Cr_2S_4$. Single crystals were obtained from a mixture of $GdCrS_3$ and Gd_2S_3 using I_2 transport. This paper presents the single crystal refinement and the magnetic properties of this compound. The structure can be described on the basis of double rutile-type chains of $[CrS_6]$ octahedra that are linked by bicapped trigonal prisms centered by Gd. This structure is reminiscent of the arrangement found in the Lillianite mineral family. © 1994 Academic Press, Inc.

INTRODUCTION

Rare earth (M) and early transition metals (T) form ternary chalcogenides with sulfur or selenium (X) with the approximate stoichiometries of MTX_3 and MT_2X_5. These compounds are layered materials that are better described with the formulation of $(MX)_n(TX_2)_m$. These phases are referred to as the misfit layered compounds (1). During the synthesis of the gadolinium misfit, $(GdS)_{1.27}CrS_2$ (2), a few crystals with a different shape were obtained. The misfit crystals are flat platelets, while these other crystals are long needles. From electron microprobe and the single crystal refinement, the stoichiometry is $GdCr_3S_6$. This phase was reported earlier by Takahashi *et al.* (3). However, the crystal structure of this compound was not determined. Along with the crystal structure, the magnetic properties are also presented.

EXPERIMENTAL

$Gd_{2/3}Cr_2S_4$ was obtained as a by-product during the preparation of the misfit derivative $(GdS)_{1.27}CrS_2$ (2). A mixture of $GdCrO_3$ and Gd_2O_3 in a 1 : 0.1 ratio was sulfurized under H_2S gas flow at 1300°C for 4 hr. $GdCrO_3$ was previously prepared by heating a Gd_2O_3–Cr_2O_3 mixture at 1300°C for 5 days. The compound powder with a small amount of iodine for vapor transport was sealed in a quartz ampoule under vacuum (2×10^{-2} atm). After annealing at 1000°C for 2 weeks, the samples were cooled to room temperature within 1 day. Both the platelets of the misfit phase, $(GdS)_{1.27}CrS_2$, and the long needles of $Gd_{2/3}Cr_2S_4$ were recovered from the low-temperature side of the tube ($T \approx 950$°C).

Semi-quantitative chemical analyses were performed using an electron microprobe (TRACOR dispersive energy model) mounted on a scanning electron microscope. The analysis results (at.% Gd = 11.0(1.5); Cr = 29.4(1.5); S = 59.6(1.5)) agree well with the expected chemical formula (at.% Gd = 10; Cr = 30; S = 60).

Weissenberg–Bragg X-ray investigations indicated that the symmetry of the structure was orthorhombic. In the Bragg photographs, the presence of weaker reflections revealed a superstructure in the **a** direction (see Photograph 1). The intensity data were therefore collected using the larger supercell; $a = 10.504(4)$ Å, $b = 10.9090(9)$ Å, $c = 12.7736(7)$ Å. These parameters are comparable to those reported by Takahashi *et al.* (3) of $a = 10.55$ Å, $b = 10.97$ Å, and $c = 12.81$ Å from powder spectra (3). The systematic extinction condition of $h + l = 2n + 1$ for the $h0l$ reflections was observed. Using this extinction, we determined the space group to be $Pmn2_1$ (no. 31).

A needle-like crystal ($1.4 \times 0.02 \times 0.012$ mm, see Photograph 2) was mounted on an Enraf–Nonius CAD4 diffractometer for data collection using Mo$K\alpha$ radiation. Unit-cell parameters were determined from a least-squares analysis of 25 reflections in the range $15° < \theta < 26°$ (CELLDIM program). Table 1 lists the conditions for data collection. The MOLEN program (Enraf–Nonius (4)) was used for data reduction, absorption corrections (DIFABS program (5) in the mode that utilizes θ-dependent systematic deviations $|F_o| - |F_c|$), structure solution, and refinement.

STRUCTURE REFINEMENT

The starting positional parameters of Gd and Cr atoms were inferred from the Patterson map. The sulfur atoms were found from subsequent Fourier-difference syntheses. The refinement was performed in the $Pmn2_1$ space group (no. 31) using full-matrix least-squares calculations. The atomic scattering factors (6) were corrected for anomalous dispersion (7). Weights were assigned according to the counting statistics (weighting scheme no. 1: MOLEN

0022-4596/94 $6.00

PHOTOGRAPH 1. The Bragg X-ray photograph of $Gd_{2/3}Cr_2S_4$ showing the a lattice spacing. The strong reflection lines correspond to the lattice spacing of $a = 3.50$ Å. The weaker reflections correspond to the 3a superstructure.

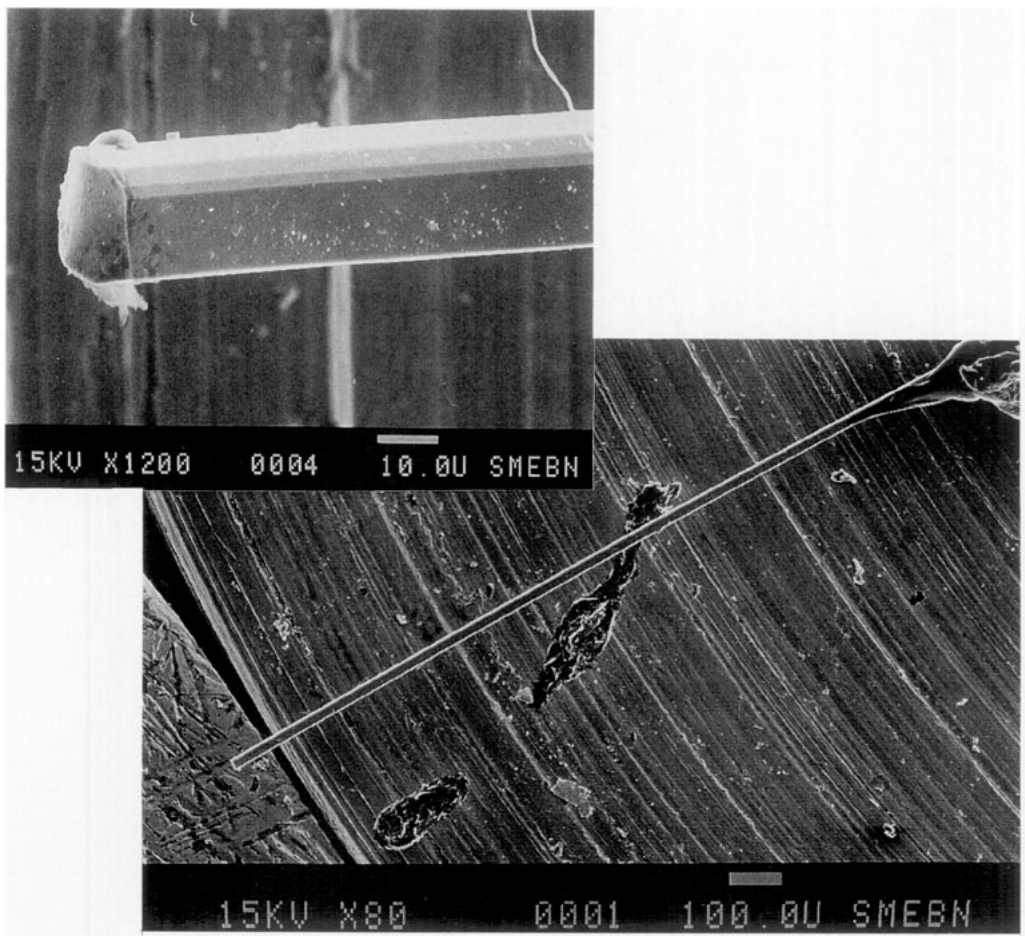

PHOTOGRAPH 2. Single crystal of $Gd_{2/3}Cr_2S_4$. The bottom picture shows the crystal magnified 80 times using 15 kV electron beam. The top picture shows the crystal magnified 1200 times.

TABLE 1
Summary of Crystallographic Data for $Gd_{2/3}Cr_2S_4$

Crystal data	
Empirical formula	$Gd_{2/3}Cr_2S_4$
Formula weight	337.1 g mole^{-1}
Crystal dimensions	1.4 × 0.02 × 0.012 mm
Cell parameters	
a	10.504(4) Å
b	10.9090(9) Å
c	12.7736(7) Å
V	1463.7(6) Å^3
D_{calc}	4.59 g cm^{-3}
Z	12
μ	147.9 cm^{-1}
Data collection	
Diffractometer	Enraf–Nonius CAD4
Radiation	Mo$K\alpha$ (λ = 0.71069 Å)
θ range for data collection	$1.5° \leq \theta \leq 35°$
h, k, l range for data collection	−16,16; 0,17; 0,20
Scan mode	ω
Scan width	1.0 + 0.35 tanθ
Max. scan time	30 sec
Structure solution and refinement (reduced cell ($a1 = a/3$) space group *Pmnb*)	
Number of unique reflections ($I \geq 1.0\ \sigma(I)$)	1120
Number of reflections (with $I \geq 2.5\ \sigma(I)$) used for final refinement	976
Number of parameters	48
Min., max. absorption correction factors	0.922, 1.177
Conventional residual	$R = 0.024$
Weighed residual	$R_w = 0.027$
Weights	$w = 4F^2/(\sigma(I)^2 + (p * F^2)^2)$
	$p = 0.03$
Extinction parameter refined	$g = 3.14(3) \times 10^{-6}$

program). The structure was refined to R/R_w of 0.037/0.039 using 1740 reflections and 105 parameters. Table 2 lists the atomic coordinates and thermal parameters.

The solution shows a statistical occupancy of the various Gd sites. Although a rather complicated distribution on the Gd sites is observed, the summation of the site occupation factors over all Gd atoms within the structure gives a chemical formulation $Gd_{2/3}Cr_2S_4$ which corresponds to charge equilibrium, i.e., Gd^{3+}, Cr^{3+}, and S^{2-}. An examination of the unit cell indicates that if the origin of the unit cell is shifted by $\Delta x = \frac{1}{4}$, $\Delta y = -\frac{1}{4}$, and $\Delta z \approx 0.17$, there exists a possible inversion center.

A refinement was conducted in the space group *Pmnb* (no. 62). This space group satisfies the centrosymmetric solution discovered above. This solution, however, has to be rejected for two reasons. First, in addition to the previous systematic absence condition ($h0l$, $h + l = 2n + 1$), a second systematic absence ($hk0$, $k = 2n + 1$) would also have to be present; however, these reflections do exist. Second, if these reflections are rejected to conduct the refinement, much higher R values are obtained ($R = 0.15$, $R_w = 0.213$ for 1693 reflections and 60 refined parameters).

So far, we have discussed a supercell approach. Now let us consider a refinement in the reduced unit cell, dividing the a parameter by three. For the conversion of data for the reduced cell refinement, all reflections with $h \neq 3n$ must be rejected due to fractional h indices. Once these reflections are rejected, the additional systematic extinction of ($hk0$, $k = 2n + 1$) is now observed. Therefore the refinement for the reduced cell was performed in the *Pmnb* space group. We choose this setting instead of the standard setting of *Pnma* so the two cells of the superstructure and the substructure can be related without a permutation of the unit-cell axes. The initial positional parameters were deduced from those listed in Table 2. A full-matrix least-squares refinement for 976 unique reflections (48 parameters; anisotropic thermal parameters for all atoms) converged to $R = 0.024$ and $R_w = 0.027$. The occupancy parameter for the Gd site was also refined (33.72(3)%). This occupancy agrees perfectly with the theoretical value of 33.3% (corresponding to $Gd_{8/3}Cr_8S_{16}$) expected from the charge equilibrium. Atomic coordinates and equivalent isotropic thermal parameters are given in Table 3a; anisotropic displacement parameters

TABLE 2
Positional Parameters and Estimated Standard Deviations
(Large Cell (a = 10.504 Å) Space Group $Pmn2_1$)

Atom	Position space group $Pmn2_1$	x	y	z	sof[a]	B_{iso} (Å^2)
Gd1	4(b)	0.32253(9)	0.48611(6)	0.5 (fixed)	0.846(2)	1.18(1)
Gd2	4(b)	0.0229(3)	0.4855(2)	0.4996(2)	0.182(1)	0.78(4)
Gd3	4(b)	0.3499(1)	−0.0125(1)	0.33935(9)	0.489(2)	0.64(1)
Gd4	*4(b)*	*0.0212(1)*	*−0.01537(8)*	*0.34107(8)*	*0.498(1)*	*0.37(1)*
Cr1	4(b)	0.3329(3)	0.3048(2)	0.2833(1)	1.0	0.77(3)
Cr2	2(a)	0	0.3027(2)	0.2870(2)	1.0	0.39(4)
Cr3	4(b)	0.3333(2)	0.3355(2)	0.7660(1)	1.0	0.66(2)
Cr4	2(a)	0	0.3393(2)	0.7681(2)	1.0	0.70(4)
Cr5	4(b)	0.3335(3)	0.8072(2)	0.5588(2)	1.0	1.01(3)
Cr6	2(a)	0	0.7984(2)	0.5580(2)	1.0	0.57(4)
Cr7	4(b)	0.3347(2)	0.8335(2)	0.0759(1)	1.0	0.69(2)
Cr8	2(a)	0	0.8360(3)	0.0735(3)	1.0	0.99(5)
S1	4(b)	0.3332(4)	0.5485(2)	0.8233(2)	1.0	0.62(3)
S2	2(a)	0	0.5541(4)	0.8265(3)	1.0	0.70(6)
S3	4(b)	0.3362(3)	0.6335(2)	0.1426(2)	1.0	0.50(3)
S4	2(a)	0	0.6296(5)	0.1408(5)	1.0	2.1(1)
S5	4(b)	0.3324(4)	0.3376(2)	0.1005(2)	1.0	0.75(4)
S6	2(a)	0	0.3443(4)	0.1025(4)	1.0	0.77(6)
S7	4(b)	0.3355(4)	0.2254(2)	0.4613(2)	1.0	0.63(4)
S8	2(a)	0	0.2037(3)	0.4544(3)	1.0	0.40(5)
S9	4(b)	0.3366(4)	0.7160(3)	0.3866(2)	1.0	0.97(4)
S10	2(a)	0	0.7127(4)	0.3880(4)	1.0	1.21(7)
S11	4(b)	0.3331(4)	0.8397(2)	0.7450(2)	1.0	0.74(4)
S12	2(a)	0	0.8421(4)	0.7408(4)	1.0	0.90(6)
S13	4(b)	0.3333(3)	0.1304(2)	0.7035(2)	1.0	0.44(3)
S14	2(a)	0	0.1285(5)	0.7012(4)	1.0	1.56(8)
S15	4(b)	0.3335(3)	0.0475(2)	0.0083(2)	1.0	0.74(4)
S16	2(a)	0	0.0529(4)	0.0120(4)	1.0	1.07(7)

[a] The definition of site occupancy factor (sof) is the average population of that site.

TABLE 3a
Positional Parameters and Estimated Standard Deviations
(Reduced Cell ($a1 = a/3$) Space Group *Pmnb*)

Atom	Position	x	y	z	sof	B_{eq} (Å^2)
Gd	8(d)	0.3003(1)	0.23603(2)	0.32983(2)	0.3372(3)	0.813(7)
Cr1	4(c)	¼	0.05407(5)	0.11305(4)	1.0	0.781(9)
Cr2	4(c)	¼	0.08554(5)	0.59579(4)	1.0	0.745(9)
S1	4(c)	¼	0.29983(8)	0.65722(7)	1.0	0.89(1)
S2	4(c)	¼	0.38116(7)	−0.03033(6)	1.0	0.85(1)
S3	4(c)	¼	0.09016(7)	−0.07136(6)	1.0	0.80(1)
S4	4(c)	¼	−0.03337(9)	0.28603(7)	1.0	1.02(1)

TABLE 3b
General Displacement Parameter Expressions ($U \times 10^4$)
(Reduced Cell ($a1 = a/3$) Space Group *Pmnb*)

Atom	$U(1,1)$	$U(2,2)$	$U(3,3)$	$U(1,2)$	$U(1,3)$	$U(2,3)$
Gd	110(3)	98.4(9)	100.1(9)	−2(1)	−8(1)	−1.7(8)
Cr1	101(3)	100(2)	96(2)	0	0	0(2)
Cr2	102(3)	95(2)	86(2)	0	0	4(2)
S1	102(4)	88(3)	150(3)	0	0	−6(3)
S2	115(4)	99(3)	110(3)	0	0	0(3)
S3	109(4)	103(3)	90(3)	0	0	−1(3)
S4	108(4)	185(4)	96(3)	0	0	28(3)

TABLE 4
Interatomic Distances in $Gd_{2/3}Cr_2S_4$ (Å)

Gd(0.30)	S1($\frac{3}{4}$)	2.7375(8)
	S1($-\frac{1}{4}$)	2.9540(8)
	S2($\frac{3}{4}$)	2.7027(7)
	S2($-\frac{1}{4}$)	2.9218(7)
	S3($\frac{3}{4}$)	2.7691(7)
	S3($-\frac{1}{4}$)	2.9833(7)
	S4a($\frac{1}{4}$)	2.997(1)
	S4b($\frac{1}{4}$)	2.924(1)
d(Gd–S)$_{ave}$		2.8812
Cr1($\frac{3}{4}$)	2 S1($\frac{1}{4}$, $\frac{5}{4}$)	2.4339(7)
	2 S3$_a$($\frac{1}{4}$, $\frac{5}{4}$)	2.4133(7)
	S3($\frac{3}{4}$)	2.388(1)
	S4($\frac{3}{4}$)	2.407(1)
d(Cr–S)$_{ave}$		2.4149
Cr2($\frac{1}{4}$)	2 S2($-\frac{1}{4}$, $\frac{3}{4}$)	2.4067(7)
	2 S4($-\frac{1}{4}$, $\frac{3}{4}$)	2.3806(7)
	S1($\frac{1}{4}$)	2.466(1)
	S2($\frac{1}{4}$)	2.381(1)
d(Cr–S)$_{ave}$		2.4036
Gd(0.20)	Gd(0.30)	0.352
Gd(0.20)	Gd(1.30)	3.8533(6)
Gd(0.30)	Cr1($\frac{1}{4}$)	3.4116(6)
Gd(0.30)	Cr2($\frac{1}{4}$)	3.5498(6)
Cr1($\frac{1}{4}$)	Cr1($\frac{3}{4}$)	3.5774(7)
Cr2($\frac{1}{4}$)	Cr2($\frac{3}{4}$)	3.5407(7)

Note. x coordinates are given in parentheses.

and interatomic distances are listed in Tables 3b and 4, respectively.

This solution appears to be quite reasonable. The Gd site occupancy ($\sim\frac{1}{3}$) is undoubtedly related to the 3**a** superstructure. However, refinements performed in the larger unit cell (3**a**) show that the framework remains unchanged and there is a complicated distribution of Gd atoms along the **a** direction (see results given in Table 2).

STRUCTURE DESCRIPTION

Figure 1 shows the projection of the reduced cell refinement onto the b–c plane. The structure of $Gd_{2/3}Cr_2S_4$ consists of staggered double columns of edge-sharing Cr octahedra. Two of these columns are highlighted in Fig. 1. The Cr–S distances within the octahedra are given in Table 4. The average Cr–S distances of 2.4 Å (see Fig. 2a) are very similar to those commonly reported. For example, Cr–S in $LaCrS_3$ is 2.396 Å. Within these double columns, Cr atoms form zigzag chains parallel to the **a** direction. The Cr–Cr distances of 3.5 Å along the **a** direction are quite comparable with those calculated between adjacent Cr atoms inside the double zigzag column; Cr1–Cr1 = 3.577 Å, Cr2–Cr2 = 3.541 Å. On both sides

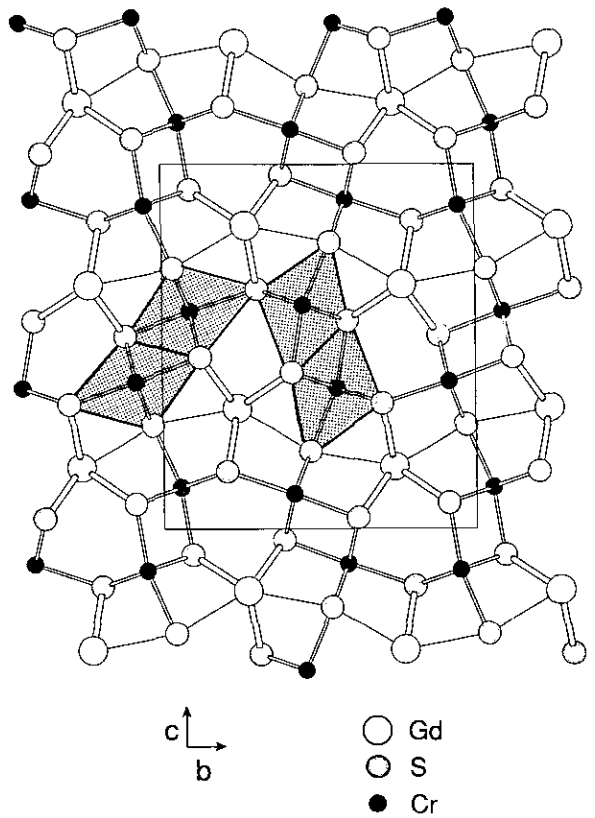

FIG. 1. The projection of $Gd_{2/3}Cr_2S_4$ onto the b–c plane. This projection is for the subcell refinement ($a = 3.50$ Å) in the *Pmnb* space group. The shaded areas correspond to the edge-sharing $[CrS_6]$ octahedra between the $[GdS_8]$ bicapped trigonal prisms.

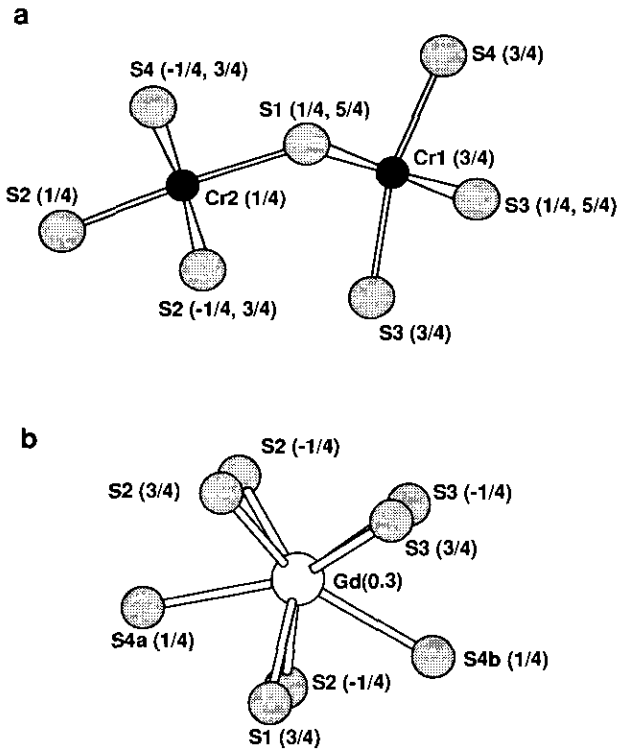

FIG. 2. The coordination polyhedra of (a) Cr1, Cr2, and (b) Gd1 atoms in $Gd_{2/3}Cr_2S_4$. The heights of the atoms in the a direction are indicated in parentheses. These atoms correspond to those listed in Table 4.

of this double column, there is a bicapped trigonal prism centered by Gd (see Fig. 2b). The Gd atoms are shifted from the ideal x positions of $\frac{1}{4}$ or $\frac{3}{4}$ causing unequal Gd–S distances inside the trigonal prism (see Table 4). Thus, Gd atoms are either above or below ($\Delta x = 0.05$) the median plane of the trigonal prism which contains the two S caps. The double column of Cr octahedra and Gd polyhedra is repeated in a serrated pattern illustrated by the bold lines in Fig. 3.

This structural pattern is also found for minerals belonging to the Lillianite family (8). Recently, Makovicky and co-workers (9) have reviewed and classified all the known members of this family. He has proposed a very simple and useful description based on an architectural concept rather than on chemical considerations. The principal structural features of the crystal structures in this family are chains of octahedra and isolated capped (mono- or bicapped) trigonal prisms. Each Lillianite homologue is classified by ^{N1,N2}L formalism, where $N1$ and $N2$ are the numbers of edge-sharing octahedra which link two trigonal prisms located in adjacent layers. Figure 4 shows some examples of this classification method for these minerals. The ^{1,2}L type is represented by Y_5S_7 (see Fig. 4a) (10). $CrEr_2S_4$ (11), $CaTi_2O_4$ (12), and $CaMn_2O_4$ (13) are examples of a ^{2,2}L case. Other more complex structure types are found in Lillianite (^{4,4}L) and Vikingite (^{4,7}L) (9). Some recent synthetic analogs which also have this type of structural motifs are $BaSm_2S_4$ (^{2,2}L) (14), $Mn_{1-x}Bi_{2+y}S_4$, and $Mn_{1-x}Bi_{2+y}Se_4$ (^{1,3}L) (15).

Although $Gd_{2/3}Cr_2S_4$ can be classified using the Makovicky formalism as a ^{2,2}L type, there exist some differences compared to the Lillianite family. First, the way $N1$ and $N2$ arms are reaching from the trigonal prisms causes a tilting of the triangular bases. In Illustration 1, the left Cr atom is at the same x level as the corner S atom, whereas on the right, Cr and S atoms' x coordinates differ by $a/2$. This results in one arm having the [CrS_6] octahedron corner sharing with the trigonal prism at this S atom and the second arm having the octahedron edge sharing with the trigonal prism.

This was not observed in the Lillianite mineral types since Cr and S atoms are located at the same x level independently of the direction (left or right) along $N1$ and $N2$ arms (see Illustration 2).

Second, the vast majority of oxides or sulfides of the ^{2,2}L type have the chemical formulation of $M^{2+}T_2^{3+}X_4^{2-}$, where M^{2+} are large eight-coordinated cations such as Ca, Sr, Ba, or Pb (within a bicapped trigonal prismatic arrangement of X atoms). Contrary to this, in $Gd_{2/3}Cr_2S_4$, Gd^{3+} is eight coordinate with a statistical occupancy of $\frac{2}{3}$ to equilibrate the charge balance. This particular point is the likely cause of the observed 3a superstructure. Even

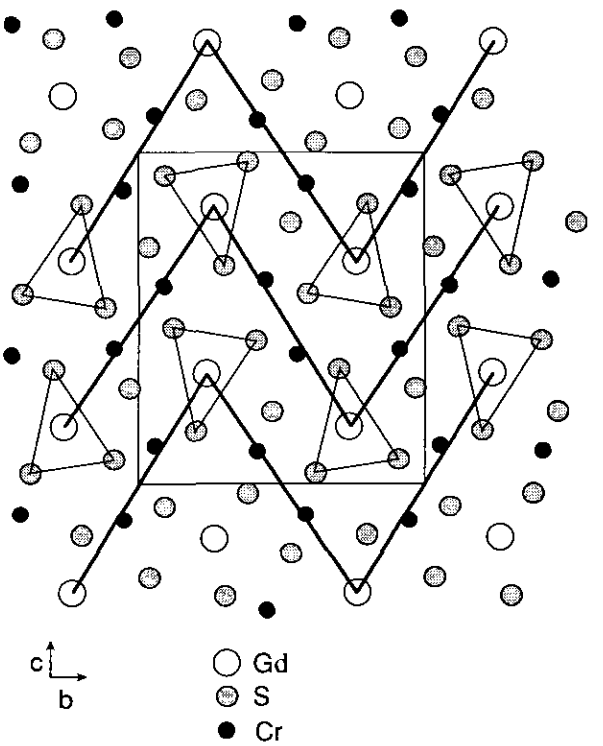

FIG. 3. The bold line indicates the zigzag pattern formed by the edge-sharing [CrS_6] octahedra (shaded in Fig. 1) and the [GdS_8] bicapped trigonal prisms. The trigonal prisms are indicated by the triangles at each vertex of the zigzag line.

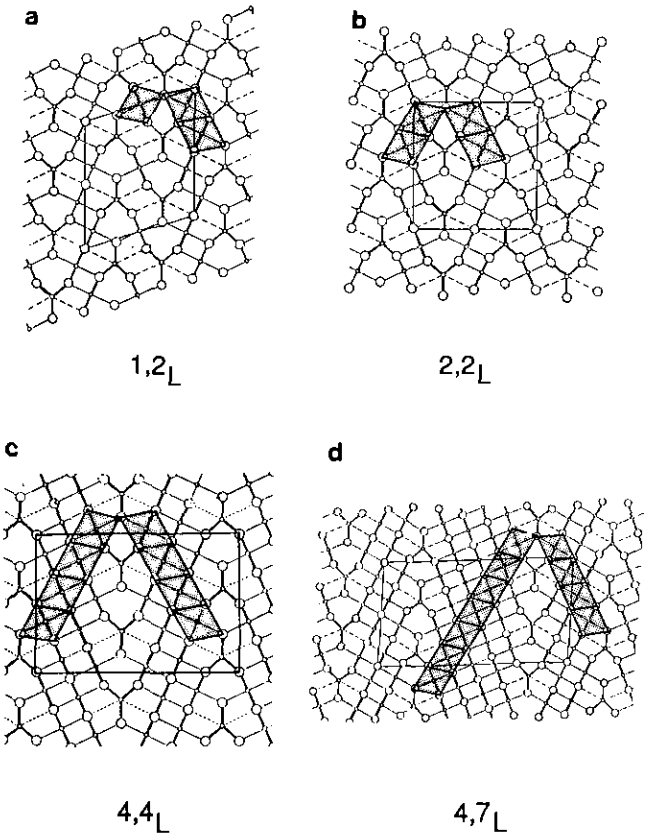

FIG. 4. Examples of the Makovicky (9) ^{N1,N2}L classification. (a) ^{1,2}L, Y_5S_7; (b) ^{2,2}L, $CrEr_2S_4$, $CaTi_2O_4$, and $CaMn_2O_4$; (c) ^{4,4}L, Lillianite; (d) ^{4,7}L, Vikingite.

if a superstructure was also mentioned for some Lillianite homologues, 3a superstructure has never been reported.

Due to the Gd site occupancy factor (sof = 0.337) one can assume that two adjacent Gd atoms are never separated by a distance of $2\Delta x$; in other words, the x, y, z and $\frac{1}{2} - x, y, z$ positions are too close to be filled simultaneously. For maximum value of sof = 0.5, the Gd should be present either at $x = 0.30$ or at $x = 0.20$ (0.70 or 0.80) but not simultaneously at the two sites. It can be concluded that the Gd atomic distribution along the **a** direction for a xyz position is a statistical one: $\frac{1}{3}$ of atomic positions occupied for $x = 0.2$, $\frac{1}{3}$ occupied for $x = 0.3$, and $\frac{1}{3}$ vacant. Figure 5 illustrates a model of this statistical distribution of Gd atoms along the **a** direction. Large differences in ionic charge favor ordering of cations, since in "defect" structure holes also tend to order.

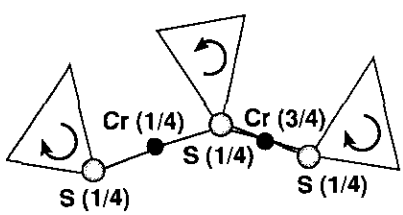

ILLUSTRATION 1

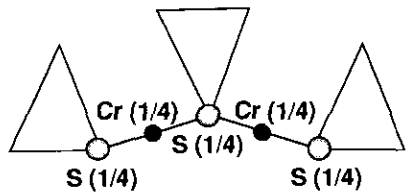

ILLUSTRATION 2

In the supercell refinement, we find that indeed the holes are partially ordering. Gd1 and Gd2 occupy the same columns parallel to the **a** direction. The occupation of these two sites suggests that the holes are found on the Gd2 site since this site is almost unoccupied. However, the other two Gd sites (Gd3 and Gd4) have a statistical occupation which is still disordered. But from this refinement, the occupation of Gd1 and Gd2 is evidence for the observed 3a superstructure.

MAGNETIC MEASUREMENTS

Magnetic properties of this phase were reported earlier by Takahashi *et al.* (3) in the temperature range 80–500 K. These authors found that the compound had Curie–Weiss behavior above 200 K, with θ_p being not far from 0 K, and a Curie constant $C_m = 15.2$ emu mole^{-1} K^{-1} (for a molecular formula of $GdCr_3S_6$). There are two points of inflection in their χ^{-1} versus T curve at low temperature. This deviation from Curie–Weiss behavior was interpreted as an antiferromagnetic ordering occurring at 143 K (as deduced from the average of the two points of inflection), although, as these authors noted, this is not a typical antiferromagnetic transition.

We have also performed a magnetic study at lower

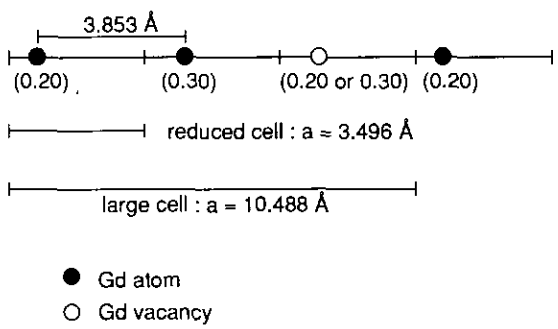

FIG. 5. Model for the 3a superstructure found in one column of face-sharing trigonal prisms in $Gd_{2/3}Cr_2S_4$. The height along the **a** direction for the reduced unit cell of each Gd is given parentheses. In the ideal 3a superstructure, two-thirds of the Gd would be occupied in this column parallel to the **a** direction. In order to have a reasonable distance between the Gd atoms, one Gd would be located at $x = 0.2$ (for the reduced cell), while in the following cell, the $x = 0.3$ would be occupied.

temperatures (2–300 K). Magnetic measurements were performed using a SQUID magnetometer device on several needle-shaped crystals ($m = 12.10 \times 10^{-3}$ g). The needle axes (which are parallel to the **a** axis) were aligned perpendicular to the applied field. The susceptibility was calculated by using the M/H ratio for one mole of $Gd_{2/3}Cr_2S_4$. Considering the high M value measured ($M > 1.10^{-4}$ emu), there was no correction applied for the diamagnetic contribution of the sample holder. After correcting for the core diamagnetism of the constituents (Gd^{3+}, Cr^{3+}, S^{2-}), the intrinsic magnetic susceptibility due to unpaired and localized electrons was calculated.

Figure 6 shows the variation of dc susceptibility as a function of temperature (χ^{-1} versus T is also shown). A paramagnetic Curie–Weiss behavior, $\chi = N\mu_{eff}^2/3k(T - \theta_p)$, is observed in the entire temperature range. A small anomaly is observed around 70 K. This anomaly does not indicate a modification of the magnetic behavior but it changes the θ_p value. The slope of the χ^{-1} vs T curve remains identical above and below this temperature anomaly. Using the high-temperature data, we find a Curie constant of $C_m = 9.2$ emu mol^{-1} K^{-1} (for a $Gd_{2/3}Cr_2S_4$ stoichiometry) with an extrapolated value of θ_p around 8 K. The observed Curie constant is in good agreement with the theoretical value of 9.0 emu mol^{-1} K^{-1} calculated from the additive contributions of Gd^{3+} and Cr^{3+} ($\frac{2}{3}$ $C_m(Gd^{3+})$ + 2 $C_m(Cr^{3+})$). However, neither the temperature onset nor the interpretation of the observed anomaly agrees with the interpretation of Takahashi. We find that this compound obeys the Curie–Weiss law down to 2 K, and do not attribute this anomaly to long-range magnetic ordering. In order to draw a definite conclusion about magnetic ordering, measurements should be performed with the crystals aligned in the other direction (i.e., the needle axis parallel to the applied field). Unfortunately, the crystals obtained were not large enough for such a measurement.

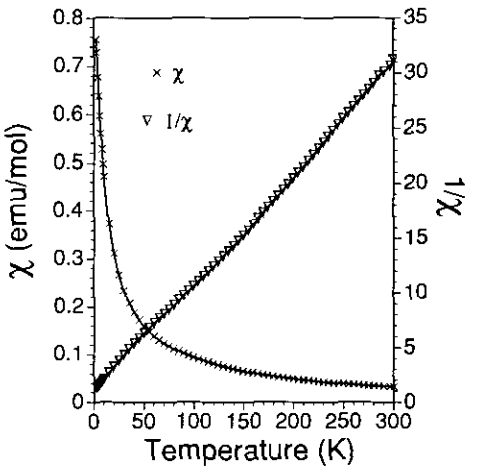

FIG. 6. The plot of the $1/\chi$ and χ versus temperature for $Gd_{2/3}Cr_2S_4$.

CONCLUSION

The structure of $Gd_{2/3}Cr_2S_4$ is reminiscent of the structure type of $CaFe_2O_4$ (16). For large A ions such as Ca^{2+} and Eu^{2+}, the AB_2O_4 oxides do not have the spinel structure. One instead observes a structure built of "double rutile" chains of BO_6 octahedra forming a 3D framework enclosing the larger A cations in a bicapped trigonal prism of oxygen atoms. As discussed above, the structure type of AB_2O_4 can be abbreviated with the Makovicky convention of ^{2,2}L. Usually, the A cation is an A^{2+} cation. In the $Gd_{2/3}Cr_2S_4$, the trigonal prismatic site is occupied by Gd^{3+}. The charge compensation is made through a statistical filling of these corresponding sites. It is likely that a variety of new ternary rare earth chalcogenides in addition to those reviewed by Flahaut (17) could be synthesized from various substitutions (not only for isoelectronic ions).

ACKNOWLEDGMENTS

We thank Y. Möelo (CNRS-Orléans) for the fruitful discussions about this structure. We also thank the CNRS for the funding of this research.

REFERENCES

1. For a review of these materials see G. A. Wiegers and A. Meerschaut, *in* "Incommensurate Sandwiched Layered Compounds" (A. Meerschaut, Ed.), Trans Tech Publ. Ltd., Zürich, 1992.
2. A. Lafond and A. Meerschaut, *Mater. Res. Bull.* **28,** 979 (1993).
3. T. Takahashi, K. Ametani, and O. Yamaha, *J. Cryst. Growth* **24,** 151 (1974).
4. C. Kay Fair, "MOLEN Structure Determination Package." Enraf–Nonius, Delft, The Netherlands, 1990.
5. N. Walker and D. Stuart, *Acta Crystallogr., Sect. A* **39,** 159 (1983).
6. D. T. Cromer and J. B. Mann, *Acta Crystallogr., Sect. A* **24,** 321 (1968).
7. D. T. Cromer and D. Liberman, *J. Chem. Phys.* **53,** 1891 (1970).
8. H. F. Keller, *Z. Kristallogr.* **17,** 67 (1890).
9. (a) E. Makovicky, *Neues Jahrb. Mineral., Monatsh.* **130,** 264 (1977); (b) E. Makovicky and S. Karup-Moller, *Neues Jahrb. Mineral., Monatsh.* **131,** 56 (1977); (c) E. Makovicky, *Neues Jahrb. Mineral., Monatsh.* **131,** 187 (1977).
10. (a) C. Adolphe, *Ann. Chim.* **10,** 271 (1965); (b) C. Adolphe and P. Laurelle, *Bull. Soc. Fr. Mineral. Cristallogr.* **91,** 219 (1968).
11. A. Tomas, Q. Chevalier, P. Laruelle, and B. Bachet, *Acta Crystallogr., Sect. B* **32,** 3287 (1976).
12. E. F. Bertaut and P. Blum, *Acta Crystallogr.* **9,** 121 (1955).
13. G. Lepicard and J. Protas, *Bull. Soc. Fr. Mineral. Cristallogr.* **89,** 318 (1966).
14. J. D. Carpenter and S-J. Hwu, *Acta Crystallogr., Sect. C* **48,** 1164 (1992).
15. S. Lee, E. Fischer, J. Czerniak, and N. Nagasundaram, *Journal of Alloys and Compounds*, in press.
16. (a) P. M. Hill, H. S. Peiser, and J. R. Rait, *Acta Crystallogr.* **9,** 981 (1956); (b) B. F. Becker and J. S. Kasper, *Acta Crystallogr.* **10,** 332 (1957).
17. J. Flahaut, "Handbook on the Physics and Chemistry of the Rare Earths" (K. A. Gschneidner and L. Eyring, Eds.), Vol. 4. North-Holland, Amsterdam, 1979.